Liquid Crystals
Publication details, including instructions for authors and subscription information:
http://www.informaworld.com/smpp/title~content=t713926090

Perturbative analysis of the nematic director reorientation dynamics induced by a magnetic field rotation in confined media

J. L. Figueirinhas[a]; J. P. Casquilho[b]
[a] CFMC-UL, Av. Prof. Gama Pinto 2, 1649-003 Lisboa Codex, Portugal and Dept. de Física, IST, 1049-001 Lisboa Codex, Portugal [b] Dept. de Física and CENIMAT, FCT/UNL, Quinta da Torre, 2829-516 Caparica, Portugal

To cite this Article Figueirinhas, J. L. and Casquilho, J. P.(2005) 'Perturbative analysis of the nematic director reorientation dynamics induced by a magnetic field rotation in confined media', Liquid Crystals, 32: 6, 727 — 734
To link to this Article: DOI: 10.1080/02678290500117761
URL: http://dx.doi.org/10.1080/02678290500117761

Liquid Crystals, Vol. 32, No. 6, June 2005, 727–734

Taylor & Francis
Taylor & Francis Group

Perturbative analysis of the nematic director reorientation dynamics induced by a magnetic field rotation in confined media

J. L. FIGUEIRINHAS*† and J. P. CASQUILHO‡

†CFMC-UL, Av. Prof. Gama Pinto 2, 1649-003 Lisboa Codex, Portugal and Dept. de Física, IST, Av. Rovisco Pais, 1049-001 Lisboa Codex, Portugal

‡Dept. de Física and CENIMAT, FCT/UNL, Quinta da Torre, 2829-516 Caparica, Portugal

(*Received 19 August 2004; in final form 6 January 2005; accepted 15 January 2005*)

We present a theoretical study of the nematic director field reorientation dynamics induced by the magnetic field rotation as a function of the magnetic field intensity, the field rotation time and the angle of rotation. A nematic monodomain sample with positive anisotropy of the magnetic susceptibility between two parallel plates with planar boundary conditions and rigid anchoring is studied. The director remains in a plane (parallel to the plates) defined by its initial orientation and the final magnetic field direction. The cases of thin and thick sample dimensions in the direction perpendicular to the director spanning plane are considered in this work. It is found that the (thermally excited) periodic modes are amplified during the director reorientation process only if the magnetic field deviates from the initial director by more than a critical angle $\alpha_c(B, \tau_r)$ where B is the magnetic induction and τ_r is the magnetic induction rotation time. In the case of large plate separation, α_c increases with increasing τ_r at fixed field and with increasing field at fixed τ_r in the range of fields studied. For the thin sample case, α_c increases with increasing τ_r at fixed field and passes through a minimum with increasing field at fixed τ_r. In both cases the wave vector increases monotonously with the magnetic field intensity at constant final field orientation α_0 and constant τ_r. At constant field and τ_r the selected mode's amplitude and wave vector increase with increasing α_0, reaching a maximum value for α_0 slightly above $\pi/2$, also in both cases.

1. Introduction

The sustained interest in self-organization phenomena in complex systems, such as the formation of periodic spatio-temporal structures on macroscopic scales in systems far from equilibrium, is related to the recognition of the similarities between the underlying dynamical instabilities in physical, chemical, biological and technological systems.

The fact that similar phenomena appear in many different systems is explained by their description in terms of non-linear partial differential equations. When a stationary solution exists, this allows the study of its stability by standard methods [1]. That is not the case reported in this work, where the system under study develops a (magnetic) field-induced transient spatial periodic pattern [2], and consequently we use a perturbation method for the study of the phenomena.

The study of the transient periodic patterns arising in the magnetically-induced reorientation of nematic liquid crystalline samples has been carried out by several authors [3]. Usually a continuous or sudden rotation of either the field or the sample are considered. When sudden rotations are considered the great majority of studies available focus on the case of a $\pi/2$ rotation angle relative to the initial director orientation, such as in Fréedericksz geometries [4–8] or in magnetic reorientation NMR experiments [9–12]. Experimental and theoretical results [2, 3, 13, 14] indicate that the periodic structures can also be present in non-orthogonal geometries. In the orthogonal geometry the periodic perturbations develop for a magnetic field above a critical value as a consequence of the degeneracy in the reorientation direction of the director back to the field direction [8]. In the non-orthogonal case the periodic perturbations are also expected when the orthogonal component of the magnetic field is strong enough, which implies the existence of a critical value for this component [13].

The theoretical studies of this situation so far are limited to sudden rotations of either the field or the sample, and do not consider the director evolution during the initial misalignment between the director and the magnetic field due to the finite rotation time τ_r. In

*Corresponding author. Email: figuei@cii.fc.ul.pt

Liquid Crystals
ISSN 0267-8292 print/ISSN 1366-5855 online © 2005 Taylor & Francis Group Ltd
http://www.tandf.co.uk/journals
DOI: 10.1080/02678290500117761

this work we consider the rotation of the magnetic field in the presence of a static sample. In the actual experiment it is easier to rotate the sample in a static magnetic field. In that case it must be checked that the nematic follows the rotation of the sample container [15]. In this study the model developed accounts for the initial misalignment process and follows the reorientation of the director back to equilibrium using a perturbation method. Our perturbation approach is consistent with the results of the optical experiments reported in [2]; when the initial misalignment between the director and the magnetic field departs significantly from $\pi/2$, the periodic structures become increasingly less visible, indicating that their amplitude is becoming very small for such angles. The numerical simulations obtained correspond to the linear mode. Only near the orthogonal condition do the amplitudes of the periodic perturbations grow sufficiently that the non-linear mode is selected and leads to the formation of the (splay–bend) inversion walls that arise in the twist Fréedericksz geometry [2].

This theoretical study considers the nematic director field reorientation dynamics as a function of the magnetic field intensity, the field rotation time and the angle of rotation. A nematic monodomain sample with positive anisotropy of the magnetic susceptibility between two parallel plates with planar boundary conditions and rigid anchoring is analysed. The director remains in a plane (parallel to the plates) defined by its initial orientation and the final magnetic field direction. Both a thin and a thick sample in the direction perpendicular to the director spanning plane are considered.

The model simulations for a 5CB nematic slab show that during the reorientation process, the (thermally excited) periodic modes are amplified during the director reorientation process only if the magnetic field deviates from the initial director more than a critical angle $\alpha_c(\tau_r)$, where τ_r is the field rotation time. Under that condition, the selected mode reaches the highest amplitude at a certain instant t_m, and the mode's amplitude and wave vector at t_m as well as time t_m are determined as a function of magnetic field intensity and final orientation α_0 relative to the initial director for a fixed τ_r. In the thick sample case, α_c increases with increasing τ_r at fixed field and with increasing field at fixed τ_r in the range of fields studied. For the thin sample, α_c increases with increasing τ_r at fixed field and passes through a minimum with increasing field at fixed τ_r; t_m decreases monotonously with the magnetic field at constant α_0 and τ_r. The wave vector increases monotonously with the magnetic field at constant α_0 and τ_r. At constant field and τ_r, the selected mode's amplitude and wave vector increase with increasing rotation angle α_0, reaching a maximum value for α_0 slightly above $\pi/2$. The maximum of both the mode's amplitude and wave vector is only reached for α_0 above $\pi/2$ because during the initial field rotation away from the director, the director partially follows the field due to the low viscosity of the nematic compound considered.

2. The model

We describe the director reorientation by a magnetic field within the context of the Leslie–Ericksen nematodynamic equations [16], considering that the director remains in the plane defined by its initial orientation (aligned with the magnetic field) and the final orientation of the magnetic field rotated of an angle α_o from its initial direction. In the model the director and velocity fields are parameterized by an ansatze that considers the reorientation process as a composition of two terms: a homogeneous reorientation with no flow associated, and a periodic perturbation which involves flow.

The director, fluid velocity and magnetic induction are respectively:

$$\begin{aligned}\mathbf{n} &= \cos[\theta(x, y, z, t)]\mathbf{e}_x + \sin[\theta(x, y, z, t)]\mathbf{e}_y \\ \mathbf{v} &= v_x(x, y, z, t)\mathbf{e}_x + v_y(x, y, z, t)\mathbf{e}_y \\ \mathbf{B} &= \mathrm{B}\{\cos(\alpha(t))\mathbf{e}_x + \sin(\alpha(t))\mathbf{e}_y\}\end{aligned} \tag{1}$$

with θ, v_x and v_y given by:

$$\begin{aligned}\theta(x, y, z, t) &= \theta_0(t)\cos(q_z z) \\ &\quad + \xi_\theta(t, \mathbf{q})\cos(q_x x + q_y y)\cos(q_z z) \\ v_x(x, y, z, t) &= -\xi_v(t, \mathbf{q})q_y \sin(q_x x + q_y y)\cos(q_z z) \\ v_y(x, y, z, t) &= \xi_v(t, \mathbf{q})q_x \sin(q_x x + q_y y)\cos(q_z z).\end{aligned} \tag{2}$$

$q_z=\pi/d$ where d is the sample thickness; $\theta_0(t)$ is the amplitude of the homogeneous reorientation; $\xi_\theta\,(t, \mathbf{q})$ is the amplitude of the periodic perturbation superimposed to it with wave vector $\mathbf{q}=q_x\mathbf{e}_x+q_y\mathbf{e}_y$. Also $\xi_v(t, \mathbf{q})$ is the velocity amplitude associated with the periodic perturbation; $\alpha(t)$ is the angle between the initial director (pointing along the x-axis) and the magnetic field, and is time-dependent during the initial misalignment between the director and the magnetic field varying from 0 to α_0 linearly in time τ_r. Starting from the director equation in the Leslie–Ericksen formulation [16] and neglecting the inertia of the director as is usually done we obtain in the mid-plane ($z=0$) the equation for $\theta_0(t)$:

$$\frac{\mathrm{d}\theta_0(t)}{\mathrm{d}t} = \frac{\chi_a B^2}{2\gamma_1\mu_0}\sin(2\alpha(t) - 2\theta_0(t)) - \frac{K_2 q_z^2}{\gamma_1}\theta_0(t) \tag{3}$$

where χ_a is the anisotropy of the magnetic susceptibility,

μ_0 is the magnetic permeability of vacuum, B is the magnetic induction, γ_1 is the director rotational viscosity and K_2 is the twist elastic constant.

Inserting **n**, **v**, and **B** in the velocity and director equations of the Leslie–Ericksen formulation [16] and keeping only the terms linear in $\xi_\theta(t, \mathbf{q})$ and $\xi_v(t, \mathbf{q})$ we obtain in the middle plane ($z=0$) the following set of first order differential equations:

$$\begin{aligned} a_{11}\frac{\mathrm{d}\xi_\theta(t,\mathbf{q})}{\mathrm{d}t}+a_{12}\frac{\mathrm{d}\xi_v(t,\mathbf{q})}{\mathrm{d}t} &= b_{11}\xi_\theta(t,\mathbf{q})+b_{12}\xi_v(t,\mathbf{q}) \\ a_{21}\frac{\mathrm{d}\xi_\theta(t,\mathbf{q})}{\mathrm{d}t}+a_{22}\frac{\mathrm{d}\xi_v(t,\mathbf{q})}{\mathrm{d}t} &= b_{21}\xi_\theta(t,\mathbf{q})+b_{22}\xi_v(t,\mathbf{q}). \end{aligned} \tag{4}$$

The coefficients a_{mn} and b_{mn} are time-dependent through $\theta_0(t)$ and $\alpha(t)$. They are complicated functions of $\theta_0(t)$, $\alpha(t)$, $\chi_a B^2$, the wave vector **q**, the three elastic constants K_1, K_2, K_3 and the five independent viscosity coefficients α_1 to α_5, and are given in the appendix. $\xi_\theta(t, \mathbf{q})$ and $\xi_v(t, \mathbf{q})$ are obtained by numeric integration of the above system using standard methods [17]. Prior to the integration of system (4), $\theta_0(t)$ has to be obtained from the numeric integration [17] of equation (3) since it enters into the coefficients a_{mn} and b_{mn}. The initial condition for $\xi_\theta(0, \mathbf{q})$ is taken from the thermal fluctuations of the director while still aligned with the magnetic field and $\xi_v(0, \mathbf{q})$ follows $\xi_\theta(0, \mathbf{q})$ adiabatically as determined by the Leslie–Ericksen equations [16]. According to the equipartition theorem $<\xi_\theta(0, \mathbf{q})^2>$ is given by:

$$\langle \xi_\theta(0,\mathbf{q})^2\rangle = \frac{4^2 k_B T}{V}\left\{\begin{array}{l} \frac{q_y^2}{q_y^2+q_z^2}\frac{1}{K_1\left(q_y^2+q_z^2\right)+K_3 q_x^2+\chi_a\frac{B^2}{\mu_0}} + \\ \frac{q_z^2}{q_y^2+q_z^2}\frac{1}{K_2\left(q_y^2+q_z^2\right)+K_3 q_x^2+\chi_a\frac{B^2}{\mu_0}} \end{array}\right\} \tag{5}$$

with $V=0.4\,\mathrm{cm}^3$ for the thick sample and $V=0.02\,\mathrm{cm}^3$ for the thin sample; k_B is the Boltzman constant and T the absolute temperature. The integration of system (4) with initial amplitude estimated from (5) up to time t is carried out as a function of **q**, and the maximum $\xi_\theta(t, \mathbf{q})$ is recorded as $\xi_\theta(t)$. The wave vector **q** that maximizes $\xi_\theta(t, \mathbf{q})$ is also recorded as $\mathbf{q}_m(t)$. One then obtains at each time t the amplitude $\xi_\theta(t)$ and the wave vector $\mathbf{q}_m(t)$ of the highest mode.

During the reorientation process, depending upon the value of α_0 and τ_r, $\xi_\theta(t)$ can evolve in different ways; when α_0 is larger than $\alpha_c(\tau_r)$, $\xi_\theta(t)$ is seen to reach a maximum amplitude at a specific time t_m and decays afterwards. In the following, the values of $\xi_\theta(t_m)$ and $\mathbf{q}_m(t_m)$ will simply be referred to as ξ_θ and $\mathbf{q}_m$. When α_0 is smaller than $\alpha_c(\tau_r)$, $\xi_\theta(t)$ is seen either to decrease monotonically from its value at $t=0$ or to go through a local maximum although inferior to $\xi_\theta(0)$ at a specific time t_m; α_c is accordingly defined as the value of α_0 for which $\xi_\theta(t_m)=\xi_\theta(0)$.

The model developed considers a finite magnetic field rotation time τ_r, and this, along with the low viscosity of 5CB, originates that the director partially follows the magnetic field during the initial field rotation of α_0, yielding an effective field rotation angle α_{eff} smaller than α_0. α_{eff} is the relevant angle in the build-up of magnetic energy in the nematic sample, and its dependence on both τ_r and the magnetic field is now analysed. For simplicity we shall restrict our remarks to the thick sample case where boundary effects can be neglected in a first approximation, and so avoiding the mathematical complications arising from taking into account the director elasticity in the case of the thin sample which is unimportant for the physical problem that we now discuss. From figure 1, we define the effective angle of rotation as

$$\alpha_{\mathrm{eff}}(t)=\alpha(t)-\theta_0(t)=\alpha_0\frac{t}{\tau_r}-\theta_0(t). \tag{6}$$

The maximum effective angle between the director and the magnetic field during the field rotation process (up to the time $t=\tau_r$) is obtained through

$$\frac{\mathrm{d}\alpha_{\mathrm{eff}}(t)}{\mathrm{d}t}=0=\frac{\alpha_0}{\tau_r}-\frac{\mathrm{d}\theta_0(t)}{\mathrm{d}t} \tag{7}$$

and using the (uniform) director dynamic equation for the thick sample case, neglecting boundary effects we obtain

$$\sin(2\alpha_{\mathrm{eff}})=\frac{2\gamma_1\mu_0}{\chi_a B^2}\frac{\alpha_0}{\tau_r}=2\frac{\tau_0}{\tau_r}\alpha_0 \tag{8}$$

from which we see that

$$\lim_{\tau_0/\tau_r\to 0}\alpha_{\mathrm{eff}}=0 \tag{9}$$

which means that the director follows instantaneously the magnetic field in the case of a very slow field

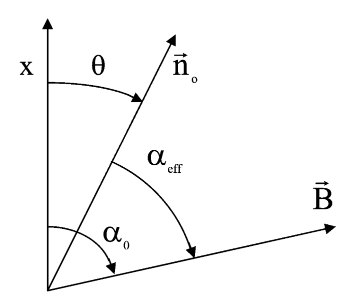

Figure 1. Schematic representation of the director and magnetic field after the initial field rotation away from the director initially along x. α_0 is the field rotation angle and α_{eff} is the effective value of the angle between the director and the magnetic field.

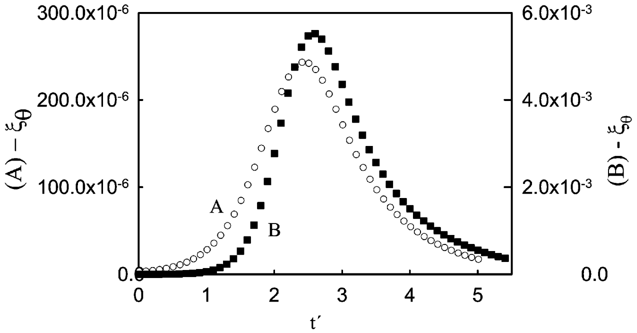

Figure 2. Time dependence of the periodic perturbation amplitude $\xi_\theta(t')$ for the thin (A) and thick (B) samples with B=0.5 T, α_0=88° and τ_r=20 ms. t' is the reduced time, $t' \equiv t\left(\chi_a B^2/\mu_0 - K_2 q_z^2\right)/\gamma_1$.

rotation or a very intense magnetic field. In the case of the thin sample similar trends for α_{eff} are expected.

3. Results and discussion

For the simulations carried out we consider the viscoelastic parameters of 5CB as given in [18] for T=299.15 K. In the simulations the thickness of the thin sample was 50 μm and the thickness of the thick sample was 1 mm.

The time dependence of the perturbation amplitude and wave vector is illustrated in figures 2 and 3 which show $\xi_\theta(t')$ and $|\mathbf{q}_m(t')|$ for the thin and thick samples as a function of the reduced time t' defined as $t' \equiv t\left(\chi_a B^2/\mu_0 - K_2 q_z^2\right)/\gamma_1$, with B=0.5 T, α_0=88° and τ_r=20 ms. The behaviour of $\xi_\theta(t')$ and $|\mathbf{q}_m(t')|$ for different values of B, α_0 and τ_r is similar to figures 2 and 3 as long as $\alpha_0 > \alpha_c$. α_c is a function of both B and τ_r, and figures 4 and 5 show the magnetic induction dependence of α_c for the thin and thick samples for

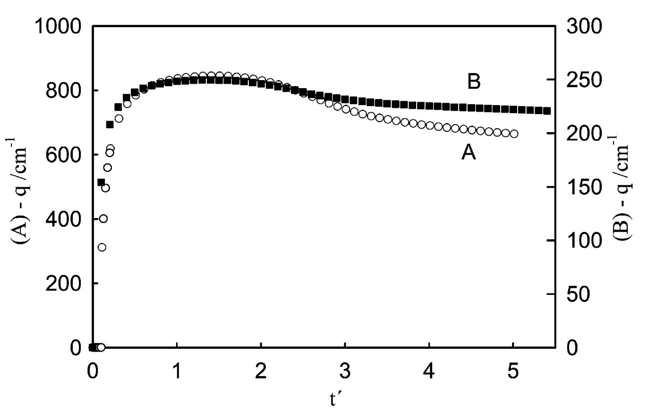

Figure 3. Time dependence of the periodic perturbation wave vector $|\mathbf{q}_m(t')|$ for the thin (A) and thick (B) samples with B=0.5 T, α_0=88° and τ_r=20 ms.

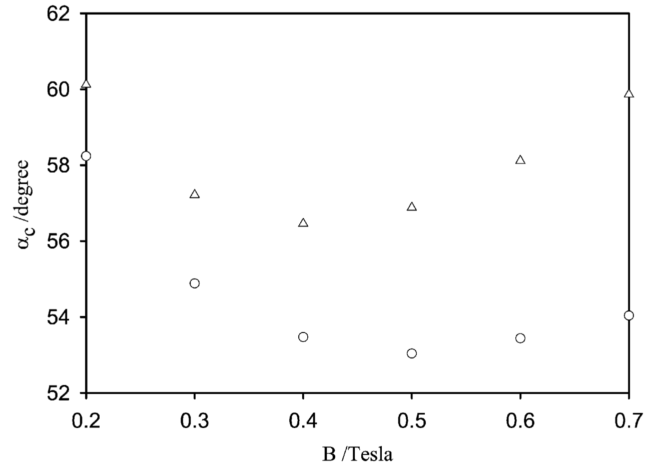

Figure 4. Magnetic induction dependence of the critical rotation angle α_c in the thin sample for two values of the field rotation time τ_r. Circles correspond to τ_r=20 ms and triangles to τ_r=40 ms.

different values of τ_r, while figure 6 gives the rotation time (τ_r) dependence of α_c in the thin and thick samples for B=0.3 T and 0.5 T.

A lower bound for α_c when τ_r approaches zero can be obtained from the dynamical stability analysis at t=0 [14]. The lower bounds for α_c obtained for the thin and thick samples and for B=0.5 T and 0.3 T are, respectively: $\alpha_c(B=0.5\,\mathrm{T},\ q_z\neq 0)=42°$, $\alpha_c(B=0.5\,\mathrm{T},\ q_z\text{–}0)=35°$, $\alpha_c(B=0.3\,\mathrm{T},\ q_z\neq 0)=47°$ $\alpha_c(B=0.3\,\mathrm{T},\ q_z\text{–}0)=35°$, which are consistent with the values reported in figure 6 for τ_r approaching 0. The increase of α_c with both τ_r and the magnetic field in the thick sample may be understood from equation (8): a larger α_0 is needed in order that α_{eff}

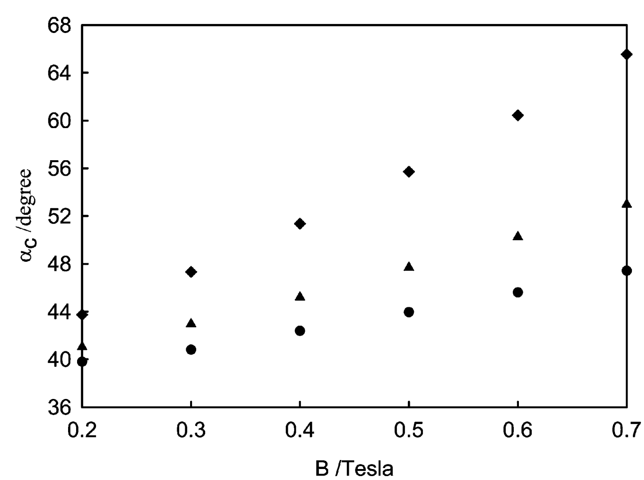

Figure 5. Magnetic induction dependence of the critical rotation angle α_c in the thick sample for three values of the field rotation time τ_r. Circles correspond to τ_r=20 ms, triangles to τ_r=40 ms and diamonds to τ_r=0.1 s.

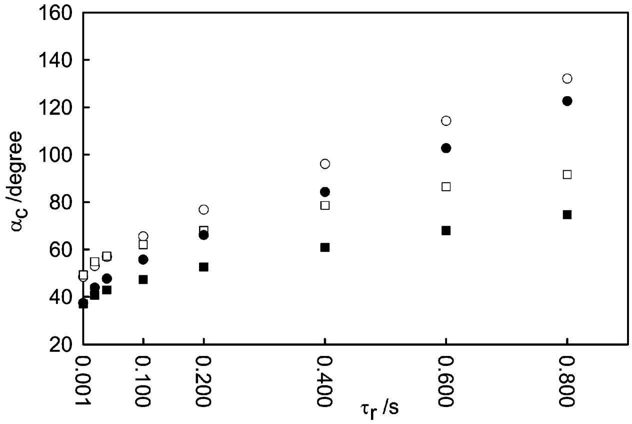

Figure 6. Field rotation time dependence of the critical rotation angle α_c in the thick and thin samples for two values of the magnetic induction. Full symbols correspond to the thick sample, squares correspond to $B=0.3$ T and circles to $B=0.5$ T.

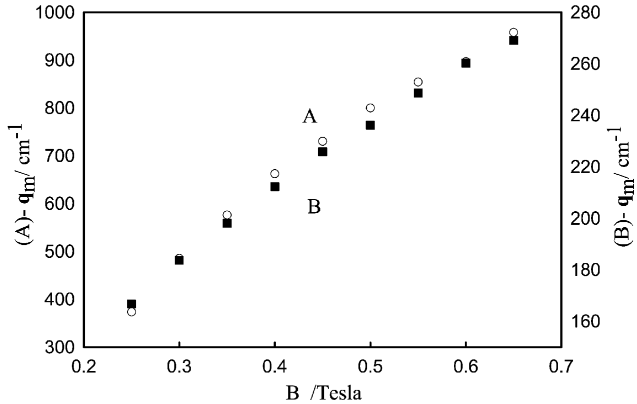

Figure 8. Magnetic induction dependence of the periodic perturbation wave vector $|\mathbf{q}_m|$ for the thin (A) and thick (B) samples with $\alpha_0=88°$ and $\tau_r=20$ ms.

attains the required value for the instability amplitude to reach, at time t_m, the same value it had at $t=0$.

The magnetic induction dependence of the perturbation amplitude ξ_θ and wave vector $\mathbf{q}_m$ for the thin and thick samples for $\alpha_0=88°$ and $\tau_r=20$ ms, is given in figures 7, 8 and 9; t_m decreases monotonously with the magnetic induction. To illustrate the α_0 dependence of the perturbation amplitude ξ_θ, wave vector $\mathbf{q}_m$ and t_m for $\tau_r=20$ ms and $B=0.5$ T, figures 10,11,12 and13 are presented. Figures 11–13 show that the transition from homogeneous to periodic reorientation is discontinuous for the above values of the control parameters. The stability analysis at $t=0$ indicates that the transition may change from discontinuous to continuous depending on the value of the reduced magnetic field [14]. The same results also indicate that for the field used in figures 11–13 the transition should be discontinuous.

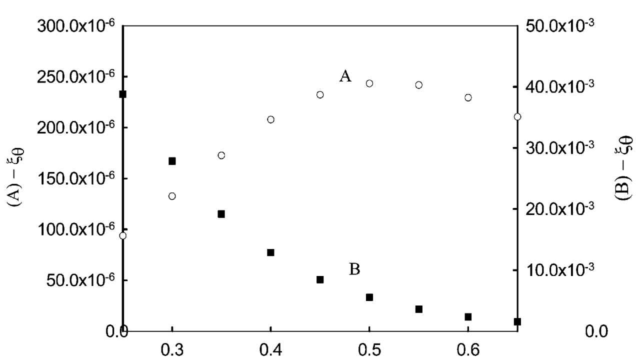

Figure 7. Magnetic induction dependence of the periodic perturbation amplitude ξ_θ for the thin (A) and thick (B) samples with $\alpha_0=88°$ and $\tau_r=20$ ms.

For α_0 in the vicinity of $\pi/2$ the perturbation approach should lose validity when the condition of the small perturbation amplitude is broken, and consequently non-linear terms should be added in order to limit the divergence of the amplitude for α_0 near $\pi/2$ (see figure 10).

In the thick sample case, α_c increases with increasing τ_r at fixed field (Fig. 6) and with increasing field at fixed τ_r (Fig. 5). For the thin sample case, α_c increases with increasing τ_r at fixed field (Fig. 6), and it goes through a minimum with increasing field at fixed τ_r (Fig. 4); t_m decreases monotonical with the magnetic field at constant α_0 and τ_r in agreement with the experimental results reported in [2]. The wave vector also increases monotonously with the magnetic field at constant α_0 and τ_r (Fig. 8) in agreement with the experimental

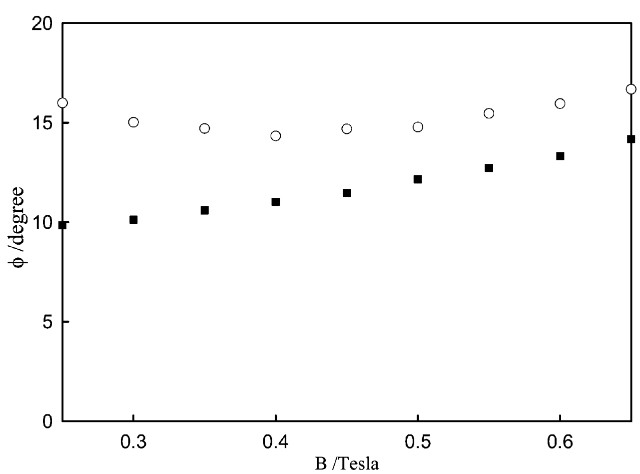

Figure 9. Magnetic induction dependence of the periodic perturbation wave vector orientation angle ϕ for the thin (circles) and thick (squares) samples with $\alpha_0=88°$ and $\tau_r=20$ ms.

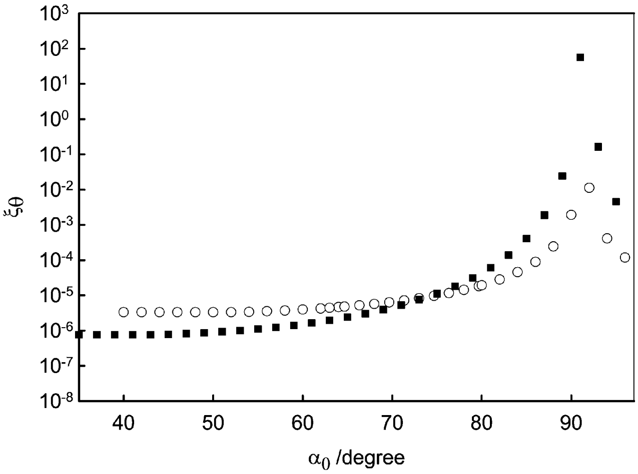

Figure 10. Field rotation angle (α_0) dependence of the periodic perturbation amplitude ξ_θ for the thin (circles) and thick (squares) samples for $B=0.5\,\mathrm{T}$ and $\tau_r=20\,\mathrm{ms}$.

results reported in [2]. The mode's amplitude passes through a maximum at a certain field for the thin sample case and decreases monotonously in the thick sample case (Fig. 7). At constant field and τ_r the selected mode's amplitude and wave vector increase with increasing rotation angle α_0, reaching a maximum value for α_0 slightly above $\pi/2$ (Figs 10 and 11). The maximum of both the mode's amplitude and wave vector is only reached for α_0 above $\pi/2$ because during the initial field rotation away from the director, the director partially follows the field due to the low viscosity of the nematic compound considered and the effective rotation angle α_{eff} becomes smaller than α_0.

Global considerations based on the magnetic energy stored in the system which is driving the reorientation process may help to clarify some of the general trends

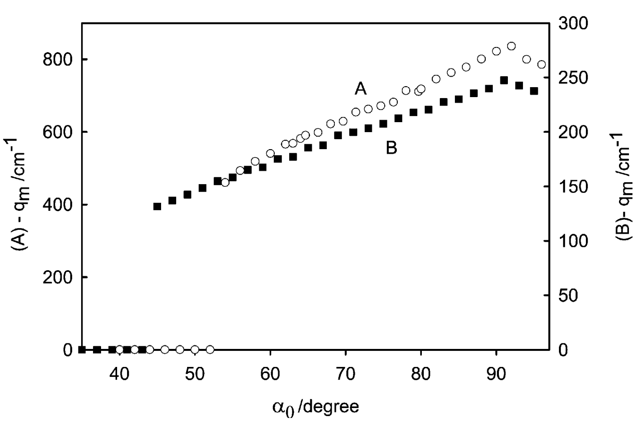

Figure 11. Field rotation angle (α_0) dependence of the periodic perturbation wave vector $|\mathbf{q}_m|$ for the thin (A) and thick (B) samples for $B=0.5\,\mathrm{T}$ and $\tau_r=20\,\mathrm{ms}$.

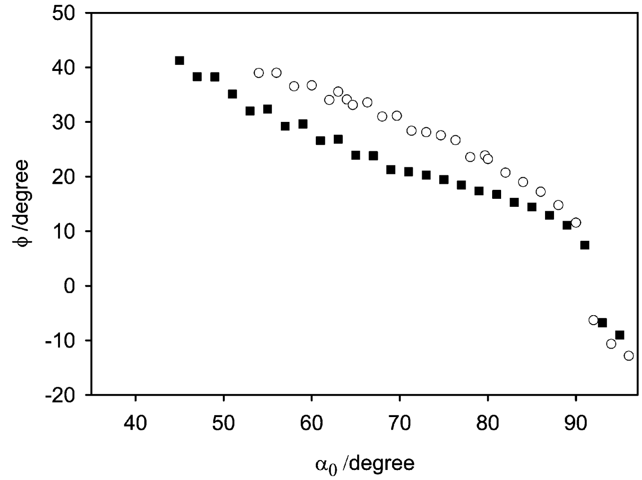

Figure 12. Field rotation angle (α_0) dependence of the periodic perturbation wave vector ($\mathbf{q}_m$) orientation for the thin (circles) and thick (squares) samples for $B=0.5\,\mathrm{T}$ and $\tau_r=20\,\mathrm{ms}$.

detected. The perturbation amplitude ξ_θ dependence on the magnetic field shows distinct behaviours for the thin and thick samples. In the thin sample, above the twist Fréedericksz critical field the perturbation amplitude increases to a maximum and decreases monotonously afterwards; in the thick sample only the monotonous decrease is evident because the maximum is attained outside the scanned field values (Fig. 7). This monotonous decrease may be associated with an increasing faster reorientation process, which cuts short the growth process of the periodic mode. The critical angle dependence on the magnetic induction also shows an

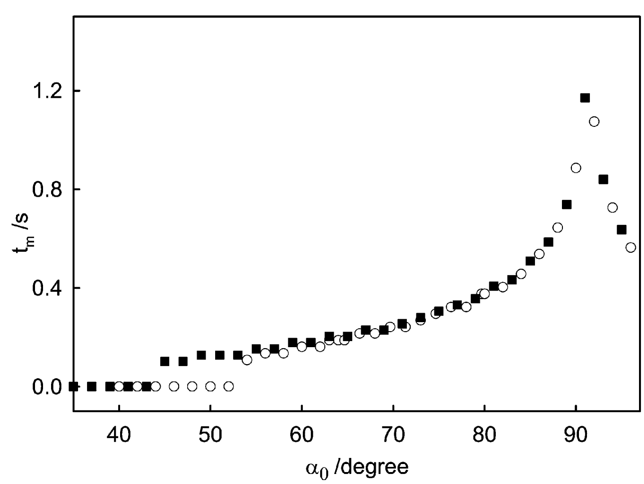

Figure 13. Field rotation angle (α_0) dependence of t_m for the thin (circles) and thick (squares) samples with $B=0.5\,\mathrm{T}$ and $\tau_r=20\,\mathrm{ms}$. For $\alpha_0<\alpha_c$, t_m refers to the homogenous mode ($\mathbf{q}=0$).

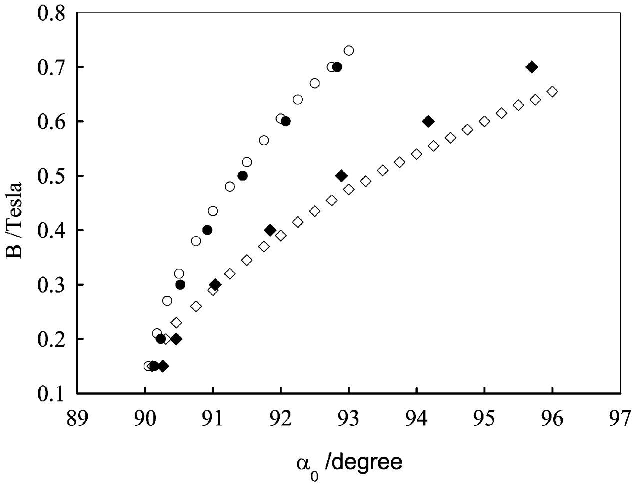

Figure 14. Relations between the magnetic induction B and the field rotation angle α_0 for zero inclination bands for two values of the field rotation time τ_r (circles—τ_r=20 ms, diamonds—τ_r=40 ms) and for the thick (full symbols) and thin (empty symbols) samples.

apparent distinct behaviour for the thin and thick sample cases (Figs 4 and 5). This arises once more due to the limited range of fields spanned, since for the thick sample case the minimum should be at a lower field than those studied, as the data for the lowest fields recorded indicates.

The wave vector increase with the magnetic field is a well known feature of the linear mode [8, 19] and traduces the existence of sufficient magnetic energy to compensate for the elastic distortion produced by a larger wave vector associated with a faster growing mode. The wave vector orientation given by $\phi=\tan^{-1}(q_y/q_x)$ is mainly dependent upon α_0 and decreases with increasing α_0; ϕ reaches 0 when $\alpha_{\text{eff}}=\pi/2$, and as a consequence of the finite field rotation time τ_r, the zero inclination ($\phi=0$) bands occur for values of α_0 and B related by the curves represented in figure 14 for different values of τ_r and for the thin and thick samples. This asymmetry in band inclination around $\alpha_0=\pi/2$ is clearly observed in the experimental results obtained in 5CB samples [2].

The monotonous decrease of t_m with the magnetic field [2] is direct evidence of a faster reorientation process as the magnetic field intensifies. The length scale of the periodic pattern is set by the cell width as expected [20].

4. Conclusions

The perturbative analysis of the director reorientation dynamics in thin and thick nematic samples for non-orthogonal geometries, presented in this work, predicts the existence of transient periodic patterns for field deviations from the initial director greater than a critical angle α_c, dependent upon the magnetic field rotation time, the final angle of rotation and the field intensity. Thermally excited periodic modes are selectively amplified during the reorientation process, reaching a maximum amplitude and later fading as predicted by an earlier analysis with τ_r=0 [3]. The selected mode only attains a significant amplitude near the orthogonal condition between the field and the initial director, in agreement with the experimental results obtained in studies with 50 μm thick 5CB nematic samples, where the periodic structures are only found in the vicinity of the Fréedericksz (twist) geometry [2].

The model predictions are in good agreement with these experimental results, in particular the predicted magnetic field dependence of the magnitude and orientation of the wave vector, and the time to reach the maximum amplitude of the perturbation, fit very well the measured values as reported in [2]. Our results show that the perturbation method that we used to study the formation of periodic stripes during the reorientation of thin and thick nematic media induced by a finite magnetic field rotation is appropriate. This suggests that this method could be used to model similar non-stationary pattern-forming phenomena in other systems.

References

[1] D. Walgraef. *Spatio-Temporal Pattern Formation*. Springer (1997).

[2] L.N. Gonçalves, J.P. Casquilho, A.C. Ribeiro, J.L. Figueirinhas. *Liq. Cryst.*, **30**, 1335 (2003).

[3] J.P. Casquilho, J.L. Figueirinhas. *Liq. Cryst.*, **29**, 127 (2002).

[4] F. Brochard, P. Pieranski, E. Guyon. *Phys. Rev. Lett.*, **28**, 1681 (1972).

[5] F. Lonberg, S. Fraden, A. Hurd, R.B. Meyer. *Phys. Rev. Lett.*, **52**, 1903 (1984).

[6] A.D. Rey, M.M. Denn. *Liq. Cryst.*, **4**, 409 (1989).

[7] U.D. Kini. *J. Phys. II Fr.*, **1**, 225 (1991).

[8] M. Grigutsch, N. Klopper, H. Scmiedel, R. Stannarius. *Phys Rev E*, **49**, 5452 (1994).

[9] A.F. Martins, P. Esnault, F. Volino. *Phys. Rev. Lett.*, **57**, 1745 (1986).

[10] P. Esnault, J.P. Casquilho, F. Volino, A.F. Martins, A. Blumstein. *Liq. Cryst.*, **7**, 607 (1990).

[11] J.P. Casquilho, P. Esnault, F. Volino, M. Mauzac, H. Richard. *Mol. Cryst. liq. Cryst.*, **180B**, 343 (1990).

[12] L.N. Gonçalves, J.P. Casquilho, J.L. Figueirinhas, C. Cruz, A.F. Martins. *Liq. Cryst.*, **14**, 1485 (1993).

[13] J.P. Casquilho. *Liq. Cryst.*, **26**, 517 (1999).

[14] J.P. Casquilho, L.N. Gonçalves, J.L. Figueirinhas. *Mol. Cryst. liq. Cryst.*, **413**, 239 (2004).

[15] C.J. Dunn, D. Ionescu, N. Kunimatsu, G.R. Luckhurst, L. Orian, A. Polimeno. *J. phys. Chem. B*, **104**, 10989 (2000).

[16] P.G. De Gennes, J. Prost. *The Physics of Liquid Crystals*. Clarendon Press, Oxford (1993).
[17] W. Press, B. Flannery, S. Teukolsky, W. Vetterling. *Numerical Recipes*. Cambridge University Press, Cambridge (1990).
[18] G. Ahlers. *Pattern Formation in Liquid Crystals*, A. Buka, L. Kramer (Eds), Chap. 5, Springer (1995).
[19] G. Srajer, S. Fraden, R.B. Meyer. *Phys. Rev. A*, **39**, 4828 (1989).
[20] P.E. Cladis, P. Palffy-Muhoray (Eds). *Spatio-Temporal Patterns in Nonequilibrium Complex Systems*. Addison-Wesley (1995).

Appendix

$$a_{11} = \alpha_3 q_x^2 - \alpha_2 q_y^2 + \gamma_2 \left[C_\theta^2 \left(q_y^2 - q_x^2 \right) - q_x q_y 2 C_\theta S_\theta \right] \quad \text{(A1)}$$

$$a_{12} = -\rho \left(q_x^2 + q_y^2 \right) \quad \text{(A2)}$$

$$a_{21} = \gamma_1 \quad \text{(A3)}$$

$$a_{22} = 0. \quad \text{(A4)}$$

$$b_{11} = 2\gamma_2\, \dot{\theta} \left[\left(q_x^2 - q_y^2 \right) C_\theta S_\theta + q_x q_y \left(1 - 2C_\theta^2 \right) \right]. \quad \text{(A5)}$$

$$\begin{aligned} b_{12} = {} & 2 q_x q_y q_z^2 (\eta_b - \eta_a) C_\theta S_\theta + q_x^2 q_z^2 \left[(\eta_b - \eta_a) C_\theta^2 - \eta_b \right] \\ & - q_y^2 q_z^2 \left[(\eta_b - \eta_a) C_\theta^2 + \eta_a \right] \\ & - q_x^4 \left\{ [\alpha_1 - (\eta_b - \eta_c)] C_\theta^2 - \alpha_1 C_\theta^4 + \eta_b \right\} \\ & - q_y^4 \left\{ [\alpha_1 + (\eta_b - \eta_c)] C_\theta^2 - \alpha_1 C_\theta^4 + \eta_c \right\} \\ & - q_x^3 q_y \left\{ 2[\alpha_1 - (\eta_b - \eta_c)] C_\theta S_\theta - 4\alpha_1 C_\theta^3 S_\theta \right\} \\ & + q_x q_y^3 \left\{ 2[\alpha_1 + (\eta_b - \eta_c)] C_\theta S_\theta - 4\alpha_1 C_\theta^3 S_\theta \right\} \\ & + q_x^2 q_y^2 \left[6\alpha_1 C_\theta^2 \left(1 - C_\theta^2 \right) + (\alpha_1 + \eta_b + \eta_c) \right]. \end{aligned} \quad \text{(A6)}$$

$$\begin{aligned} b_{21} = {} & q_x^2 \left[(K_3 - K_1) C_\theta^2 + K_1 \right] + q_y^2 \left[(K_1 - K_3) C_\theta^2 + K_3 \right] \\ & + q_x q_y 2 (K_3 - K_1) C_\theta S_\theta + h_0^2 [\cos(2\theta - 2\alpha)]. \end{aligned} \quad \text{(A7)}$$

$$\begin{aligned} b_{22} = {} & q_x^2 \left[\gamma_2 C_\theta^2 - \alpha_3 \right] + q_y^2 \left[-\gamma_2 C_\theta^2 + \alpha_2 \right] \\ & + q_x q_y 2 \gamma_2 C_\theta S_\theta \end{aligned} \quad \text{(A8)}$$

In these equations we have used the notation

$$C_x \equiv \cos x, \; S_x \equiv \sin x$$

and the definitions

$$\gamma_1 = \alpha_3 - \alpha_2, \; \gamma_2 = \alpha_3 + \alpha_2, \; \eta_a = \frac{1}{2}\alpha_4$$

$$\eta_b = \frac{1}{2}(\alpha_3 + \alpha_4 + \alpha_6), \; \eta_c = \frac{1}{2}(\alpha_4 + \alpha_5 - \alpha_2), \; h_0 = \left(\frac{\chi_a}{\mu_0} \right)^{\frac{1}{2}} B.$$